SEMARAK ILMU PUBLISHING

Semarak International Journal of Material Research

Journal homepage:
https://semarakilmu.my/index.php/sijmr/index
ISSN: 3083-8908


# Deproteinised Natural Rubber (DPNR) Wear Phenomenon on Minimum Quantity Water Lubricated (MQWL) Conditioning Study

Ramdziah Md. Nasir[1,*], Nur Aqhira A. Merican[1], Muhamad Fitri Adnan[2]

[1,] Nano Fabrication and Functional Lab, School of Mechanical Engineering, Engineering Campus, Universiti Sains Malaysia, 14300 Nibong Tebal, Pulau Pinang, Malaysia
[2] Automotive and Applied Thermo Lab, School of Mechanical Engineering, Engineering Campus, Universiti Sains Malaysia, 14300 Nibong Tebal, Pulau Pinang, Malaysia

**ARTICLE INFO**

***Article history:***
Received 9 October 2025
Received in revised form 19 February 2026
Accepted 2 June 2026
Available online 8 June 2026

A Minimum Quantity Water Lubricated (MQWL) approach (0.0–10.6 ml) was applied to investigate the abrasive wear behaviour of deproteinised natural rubber (DPNR) under sliding conditions. Pin-on-disc (PoD) tests were conducted under controlled loads (5–25 N), sliding speeds (0.26–1.31 m/s), and sliding distances (78.54–392.70 m). The term critical operating condition refers to the highest stable load–speed combination at which continuous sliding was maintained without excessive specimen deflection or loss of contact. Catastrophic wear is defined as sudden material failure characterised by severe deformation, chunk detachment, and abrupt termination of the test. DPNR-25 (25 pphr. carbon black) reached its critical operating condition at 15 N and 0.79 m/s, whereas DPNR-50 (50 pphr. carbon black) withstood higher loading and exhibited catastrophic wear only at 25 N and 1.31 m/s. Under MQWL conditions, DPNR-25 showed a 30% improvement in wear resilience compared with its unlubricated baseline, while DPNR-50 exhibited a further 58% improvement relative to DPNR-25 under identical lubricated conditions, achieving a minimum specific wear rate of 0.05 $mm^3/N{\cdot}m$. Scanning electron microscopy (SEM) and energy-dispersive X-ray (EDX) analysis were used to elucidate wear mechanisms. Finite element analysis (FEA) was employed as a qualitative, tyre-scale simulation to assess deformation trends and safety margins under high load conditions, bridging laboratory-scale wear observations with realistic tyre operating scenarios.

***Keywords:***
Tribology; DPNR; carbon black, MQWL, FEA

## 1. Introduction

Over the years, rubber abrasion has been one of the most crucial properties for rubber products, especially tires. However, rubber abrasion continues to be a highly significant challenge in rubber research. Most literature reviews are lacking on focusing the effects of the rubber abrasion for both lubricated and unlubricated conditions. Therefore, the main objective of this present paper is to study the effects of the rubber abrasive wear in lubricated environments. It has been reported that the tribological properties are observed and measured meticulously to increase the usage of the rubber material in large [1]. Rubber is a particularly valuable material in a variety of industrial applications due to its good grip, sealing, and cushioning qualities. Rubber has several very practical characteristics, including a high Poisson ratio, a big elongation-to-break, and a low Young's modulus,

which make it appropriate for numerous sealing applications in a variety of machinery and appliances [2].

A schematic relationship between the terms of tribology, wear, abrasion, and scratch etc. has been reported [3]. In general, wear can happen in a variety of places and objects relative to time. Abrasive wear mechanisms are the primary cause of material degradation. Material displacement and removal due to abrasion between two hard asperities on one or both movable surfaces are known as abrasive wear. Since abrasion is the cause of 50% of all wear issues in industry, much laboratory research has been conducted to justify the abrasive wear behaviour of a variety of unconventional and advanced materials. Although there are various research and studies that have been done regarding the wear behaviour of the rubber components, most of them are simply concerned with certain rubber products such as styrene butadiene rubber (SBR) that is widely used in manufacturing tire treads for cars [4,9,14]. Others have reported on the shoe's soles, tire treads, conveyor belts, and annular blow-out preventers that seal oil drilling pipes are examples of rubber applications that commonly experience abrasion [5,10,18,23,26]. It is one of the most crucial characteristics of a rubber material because it frequently influences the lifespan of a product. An automobile driven with inadequate tire tread depth may rupture or skid off the road because of failure due to abrasion [6]. Understanding the friction and wear characteristics of tire tread rubber is crucial to enhancing vehicle safety since styrene butadiene rubber (SBR), the primary component of tire treads, is widely employed in the rubber industry. Friction and tire wear on moving objects are mostly caused by abrasive processes, particularly local slip [7].

In tire applications, Natural Rubber (NR) has weak oil resistance but good mechanical qualities and heat build-up. It has been exploited and made commercially available in a range of manufacturing items, including tires, O-rings, gaskets, bumpers, and fenders [8]. According to the above studies, rubber could be said as one of the important products in the market especially in automobile industries. Therefore, in designing rubber products, it is crucial to consider the friction and wear behaviour of the rubber characteristics. In this study, the use of numerical approach in investigating the rubber behaviour along with an appropriate experimental design in disseminating data was conducted. The implemented simulations through three-dimensional finite element analysis (FEA) modelling to investigate the effects of particle type, size, and concentration on scratch behaviour of multiphase polymeric systems has been discussed [7]. A certain level of accuracy in the correspondence between relations in the simulating device and relations in the target for simulations has also been studied. Therefore, it is crucial to conduct experiments to confirm that the results of the simulations are accurate. Researchers also evaluated the mechanical qualities of four distinct types of elastomeric mounts with varying amounts of CB loading. The study found that raising the CB percentage increased the static stiffness of all types of elastomeric mounts. Furthermore, the addition of CB to the NR compound may result in a significant impact on the tensile strength of the rubber compound [9]. The common type of abrasive wear resulting from friction between moving parts and rigid materials such as in conveyor belt systems are longitudinal scratches and micro-cutting mechanisms. Two-body abrasive wear, three-body abrasive wear, and a combination of both are also considered as different types of abrasive wear [10]. More research has been done on two-body abrasion of polymeric wear materials than three-body abrasive wear by different investigators [10-12]. By relating rubber abrasion resistance to its mechanical characteristics, it is possible to predict a product's service life and to build lab scale abrasion test methods in accordance. Some research has described the types of rubber abrasive wear and their patterns. For instance, Schallamach was the first to investigate rubber failure by moving a hard protrusion across its surface [3,13]. In this case, rubber abrasion is investigated utilizing a controlled-environment needle scratching of the surface. Rubber abrasion is described as a mechanical

breakdown that produces a periodic surface pattern called an "abrasion pattern," also known as Schallamach's waves. Rubber is viscoelastic, yet it does not return to its exact or initial position due to this property. Wear rate is not constant until a stable pattern is developed because abrasion rate rises with the gradual development of a wear pattern [14].

A third body is also present in a three-body abrasion scenario, and it is made up of interfacial materials that were either produced naturally or were brought into the system, such as wear debris, lubricants, entrained particles, or even reactive chemicals. In a study by Hakmi *et al*., [10] and Molero *et al*., [13], the wear patterns of conveyor belts made of rubber with two and three bodies (ISO (International Student Orientation) 4649 and ASTM G65) were compared. Abrasion was not present in the rim region, and the cracks were attributed to oxidative hardening and continual toughening. The surface was extremely smooth and showed obvious signs of abrasion wear, but there was no crack in the centre area. The central abrasion rates are greater than the rate of crack propagation, preventing the development of bigger cracks [14]. This phenomenon is also particularly interesting in our study as the similar occurrence could be observed in the tires wear mechanisms. Other research has focused on the technical and environmental aspects of tire shredding focusing on contact with ground application [15]. Both processes—adhesion and hysteresis—are responsible for the stick-slip action that occurs between rubber and counter surfaces. The former is a bulk occurrence within the rubber's own body, while the latter causes it to stick to the surfaces. There are various unique wear mechanisms, such as abrasive wear, fatigue wear, and roll formation, depending on the state of the counter surface texture. The first two types typically occur on rough and blunt surfaces, but the last type occurs for comparatively smooth and soft elastomers and on smooth abrading surfaces. An adhesion mechanism that causes wear by roll could be created by rubbing against a smooth material. Because the rubber has a low rip strength, rubbing against a relatively smooth texture could result in an adhesion mechanism where wear is caused by the development of rolls. In addition, it was demonstrated that the wear process changed as rubber's elastic modulus increased, moving from fatigue wear to wear by roll formation and then to abrasive wear. When rubber is rubbed against a rough surface, the adhesion mechanism causes a cutting wear mechanism to exert abrasive action as mentioned by Motorcycle Dynamometer [16], F1 tires [17] and Wu *et al*., [18].

The tribological performance of rubber materials is critically important in applications such as tyres, seals, and conveyor systems, where friction and abrasion directly influence service life and safety. While extensive studies have examined rubber abrasion under dry conditions, comparatively fewer investigations address lubricated or minimally lubricated environments that more closely resemble real road conditions, particularly under wet or water-assisted cooling scenarios.

In the present work, a laboratory-scale pin-on-disc (PoD) configuration is employed to characterise the abrasive wear behaviour of deproteinised natural rubber (DPNR) compounded with different carbon black (CB) loadings under minimum quantity water lubrication (MQWL). The PoD test provides controlled, repeatable material-level wear data, enabling systematic evaluation of load, speed, and lubrication effects. However, PoD testing alone cannot directly represent full-scale tyre behaviour due to geometric, contact, and loading scale differences. To address this limitation, finite element analysis (FEA) is introduced as a complementary, qualitative tool. The FEA does not aim to replicate PoD wear rates, but rather to provide insight into deformation behaviour, load-bearing capability, and safety margins of a tyre-scale rubber structure under high loading conditions. This combined experimental–numerical approach enables a clearer linkage between laboratory tribological behaviour and real tyre performance trends. PoD experiments provide material-level tribological parameters, while FEA serves as a qualitative, tyre-scale validation tool to assess deformation trends and safety margins under realistic loading. FEA is not intended to directly

replicate PoD wear rates, but rather to bridge laboratory-scale abrasion behaviour with real tire operating conditions such as load-induced deformation and contact stress distribution.

## 2. Materials and Methods

### *2.1 Materials*

Deproteinised natural rubber (DPNR) were supplied by Malaysia Rubber Board (MRB) Pte. Ltd. and Carbon Black (CB) by Sigma-Aldrich, USA, <1 mm, 99.9%. The DPNR rubber was fabricated in a way that is usually described in the literature and standardized by Malaysia Rubber Board (MRB) in the form of slab rubber of dimensions 150 mm x 75 mm x 25 mm. The rubber was formulated and vulcanized from pre-deproteinised natural rubber with the conditions as listed in Tables 1 and 2. Two samples of deproteinised natural rubber (DPNR) were used in this experiment, which are DPNR-25 (batch number BG840/2/25) and DPNR-50 (BG840/3/50) whereby numbers 2 and 3 referring to production masterbatch numbers, respectively) with two different carbon fillers i.e. 25 pph. and 50 pph. rubber, respectively. The mechanical testing was done at MRB laboratory, and the typical mechanical results are as shown in Table 3. Rubber slab was cut using a special cutter for DPNR i.e. 10-inch table band saw. 30 rubber specimens were cut according to the size requirements for the tribological tests i.e. 10 mm x 10 mm x 35 mm. The rubbing face of the block rubber is 10 mm x 10 mm. A total of 60 samples of rubber block for both types of rubber is used in this experiment according to the desired parameters for each sample, as shown in Figure 1.

**Table 1**
Formulation of DPNR/HCB 25 and DPNR/HCB-50

| **Compounding ingredients** | **Formulation part per hundred (pphr)** | |
|---|---|---|
| **Rubber** | **DPNR/HCB-25** | **DPNR/HCB-50** |
| DPNR | 100 | 100 |
| Zinc oxide | 3 | 3 |
| Stearic acid | 2 | 2 |
| Black ISAF 220 | 25 | 50 |
| Permanax TMQ | 2 | 2 |
| Santoflex 13 | 2 | 2 |
| Master batch | 134 | 159 |
| Sulphur (vulcanization agent) | 1.5 | 1.5 |
| CBS (accelerator) | 1.5 | 1.5 |

**Table 2**
Vulcanisation conditions for pre-mix deproteinised natural rubber

| | |
|---|---|
| Fill Factor | 0.7 |
| Rotor speed, rpm | 100 |
| Starting temperature, $^{o}$C | 70 |
| Mixing cycle | Time of adding ingredients in Banbury internal mixer (Model BR1600) in min |
| Insertion of rubber (100 wt.%DPNR) | 0 |
| Mixing cycle | Time of adding ingredients in Banbury internal mixer (Model BR1600) in min |
| Insertion of rubber (100 wt.%DPNR) | 0 |
| Insertion of pre-mix powder ingredients (3wt.% ZnO, 2wt.% stearic acid, Permanax TMQ, Santoflex 13, 1.5wt.% Sulphur, CBS and balance wt.% master batch | 0.5 |
| Addition of half black (C-black ISAF220 hard) | 1 |
| Addition of second half of the C black | 1.5 |

| | |
|---|---|
| Sweep | 2.5 |
| Dump | 3.0 |
| Vulcanisation temperature, °C | 140 (with C black 150) |
| Hydraulic pressure for hot press process, MPa | 45 |

**Table 3**
Typical mechanical properties of DPNR 25 and DPNR 50*

| Property | DPNR 25 | DPNR 50 |
|---|---|---|
| Tensile strength, MPa | 85 | 87 |
| Modulus at 100%, MPa | 86.5 | 88.5 |
| Modulus at 300%, MPa | 91.3 | 93 |
| Elongation at break, % | 600 | 640 |
| Hardness, IRHD | 61.8 | 62.1 |
| Aged for 3 days @100 °C (% retention | | |
| Tensile strength, MPa | 87 | 89 |
| Modulus at 100%, MPa | 111 | 113 |
| Modulus at 300%, MPa | 82 | 95 |
| Elongation at break, % | 490 | 510 |
| Hardness change, IRHD | +3.5 | +3.0 |
| Aged for 3 days @100 °C (% retention | | |
| Tensile strength, MPa | 87 | 89 |
| Modulus at 100%, MPa | 111 | 113 |
| Modulus at 300%, MPa | 82 | 95 |
| Elongation at break, % | 490 | 510 |
| Hardness change, IRHD | +3.5 | +3.0 |
| Modulus of resilience (MR 100%), $N/mm^2$ | 1.2 | 1.6 |
| Compression set 24hr at 70 °C | 23.9 | 25.1 |
| Resilience (Dunlop) at 23 °C, % | 69.7 | 68.8 |
| Trouser tear, $N/mm^2$ | 10.3 | 9.7 |

*Mechanical testing at MRB

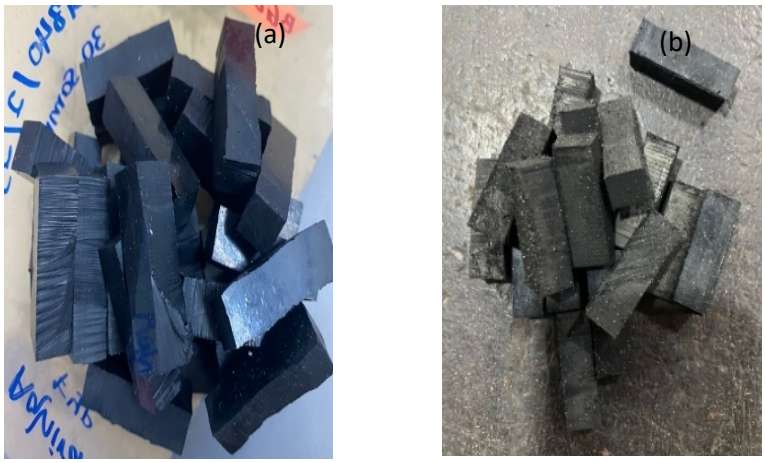


**Fig. 1.** Samples were cut using a special cutter for (a) DPNR-25 and (b) DPNR-50

Initial and final weights were taken for each of the samples before and after the test using a digital electronic balance (SHIMADZU AUW220D) with an accuracy of 1 mg. The volume was also recorded using the water displacement method.

### *2.2 Tribological Testing*

For tribological data, the DUCOM Pin-On Disc (POD) tester, type TR-20, was used to study wear and abrasion according to ASTM G99. The DPNR sample was held in a specimen holder with a diameter of 10 mm during the preparation of the testing sample. Stronghold superfine abrasive paper with high grain (Diamond 600) grade 600 abrasive paper with particle size of p1000 (average 10.6 microns or 0.0106 mm) was adhered to a steel rotating disc. The wear track diameter was adjusted to 50 mm and screwed firmly to avoid movement and slippage. A dead weight loading method would be used to load the sample from 5 N (0.05MPa) up to a maximum of 30N (0.3MPa) against the disc. All rubber samples were to undergo a 5-minute tribological test at various rotational speeds between 0.26 and 1.31 m/s with a standard load and the data was recorded using a WINDUCOM 2010 desktop software.

The amount of water used (ranging from 0.0 to 10.6 ml) in each sample was taken during the experiment where it was measured using a syringe in millilitres. As the rubber samples started rotating on the abraded surfaces, water was dropped near the samples until the time was finished at 300sec or less based on the maximum allowable abrasion before slippage or catastrophic wear occurred. The total amount of water used is added up after the end of each experiment. All the parameters used are shown in Table 4.

**Table 4**
Set up parameters

| **Parameters** | **Values** |
|---|---|
| Load (N) | 5 – 30 |
| Norminal contact pressure (MPa) | 0.05-0.30 |
| Speed (m/s) | 0.26-1.31 |
| Sliding distance (m) | 78.54-392.70 |
| Time taken (minutes) | 5 |
| Amount of water used (ml) | 0.0 – 10.6 |

After tribo-testing, each sample was examined using Scanning Electron Microscopy (SEM; Hitachi S3400N) to determine the morphology of the worn surface and the Energy Dispersion X-ray (EDX) analysis was performed to determine the elemental composition of the sample.

### *2.3 Simulated Model*

Abaqus FEA version 12 software has been used to simulate a tire rolling interacting with the asphalt road surface and a model of bike chassis dynamometer was chosen. A rolling road, used to simulate various road conditions using one or more fixed roller assemblies in a controlled environment. The simulation is used for a variety of vehicle testing and development in designing processes. The difference in this study model is the usage of rotating cylindrical model plane as reference to ensure the tire would roll for a long session rather than the normal linear model plane to measure torque and horsepower of vehicle during simulation. In this study, only the roller is modelled, hence, the dynamometer frame and the roller specification were based on its manufacturer on a website page as reference (Motorcycle Dynamometer |Hyper Power, n.d.) in creating a chassis dynamometer roller was followed [16].

Specifications used are single roller (SR): roller diameter: 325 mm; roller weight: $\pm 300\ kg$; roller inertia:$6.6\ kgm^2$; roller linear mass simulation: $200\ kg$ ; maximum wheel track: $500\ mm$; maximum allowable speed:$330\ km/h$ ; maximum power absorption: $370\ kW (500\ HP)$ (depending on the

wheels spin); maximum tractive effort: $4000\ N$ (depending on wheel spin); and roller knurled.

A basic early used tire with no tread is created to ensure simulation results depict average tire reaction. The simulation is focusing mainly on tire behaviour; therefore, wheel rim modelling was served as a load transfer medium. In this simulation, the wheel model used as a reference was the model depicted from a real-life working wheel as shown in Figure 2(a). However, the rim of the tire was changed to Honda Rs150r model as mentioned earlier because the tire mechanical functionality is complicated as shown in Figure 2(a) and (b). A moped rim was used as a reference to ease the process of modelling as shown in Figure 2(c)[17]. SolidWorks was used to model the simulation entity prior to usage of Abaqus FEA (formerly ABAQUS). Most of the simulations were based on an aircraft modelling of its tires fatigue wear [18]. The rim of a moped motorcycle Honda Rs150r was used as a reference model considering its availability nearby. As for the tire modelling, with the largest possible size being 14 inches, a Suzuki VS125 was referred. Due to software limitations, a simple scaled down model with a maximum of 1000 nodes were chosen. At first, the wheel is created on SolidWorks in Solidpart (SLDPRT) language before converted to STEP format used in Abaqus software. The modelled rim and tire are then imported into Abaqus by importing the file with compatible source software and the target software.

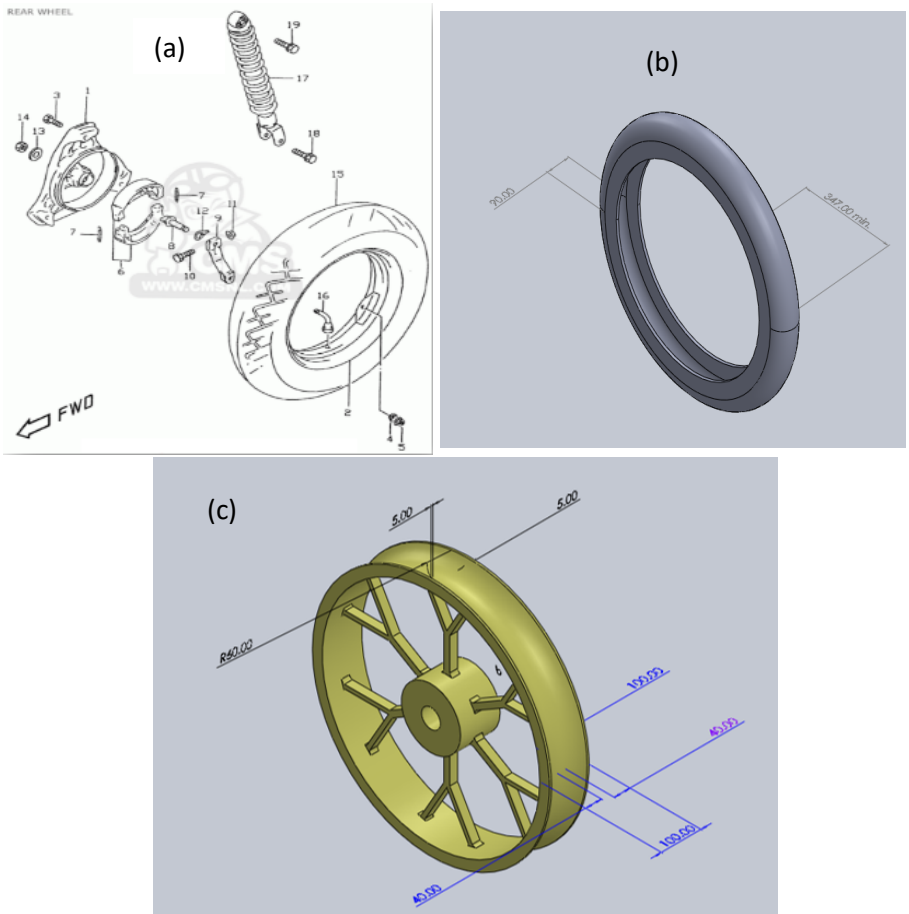


**Fig. 2.** The assembly of (a) Wheel Model of Suzuki VS125(b) Tire Model Dimension (3D Isometric) with all dimensions in mm (c) Rim Model (F) (in mm)

Creating and interfacing were done by choosing appropriate command from the software library to simulate their property including mass density, Young's modulus, and Poisson ratio. For this model, 3 properties are needed, including rim, tire, and roller assignment of material, which was

referred from various sources as shown in Table 5.

**Table 5**
Pre-set property for tire components

| Model | **Property** | **Sources** |
|---|---|---|
| Tire | Stydiene – butadiene rubber | (Styrene-Butadiene Rubber \| Designerdata, n.d.) similar property with DPNR50 (Tyre Wear: Tyre and Particle Composition, n.d.) |
| Rim | Alloy A356 | (What Is A356 T6 Aluminum Alloy \| JC Metal, n.d.) |
| Roller | Bitumen | (Asphalt Concrete \| Density, Strength, Melting Point, Thermal Conductivity, n.d.) |

The time increment in Abaqus Explicit was set to 0.1 millisecond. For an all-inclusive surface such as exterior faces, shell perimeter edges, edges based on beams and trusses, and analytical rigid surfaces in the model, general contact interactions are typically defined. When assigning interactions in Abaqus finite element analysis (FEA), it involves selecting the appropriate interaction types, such as frictionless contact, tied or bonded behaviour, including the type of contact (e.g., point, surface, or edge contact) and the contact algorithm.

The tangential frictional models and normal riding behaviour in which the contact toward asphalt material was considered to affect the tire performance. Surface–to–surface contact i.e. the collision of two different materials was created which depicts the interaction property. Mechanical properties were included in selecting normal behaviour which give the interaction the behaviour during vertical collision with the roller. In the boundary condition, mechanical displacement or rotation distribution was specified as U1(depicts force on X-axis), U2(Y-axis), U3(Z-axis), UR1(depicts the rotation on X in radian per second), UR2 (rotation on Y) and UR3(rotation on Z) and amplitude ramp (speed in rpm) respectively were referred to as the directions of motion for running the simulation concurrently. Finally, validation of load data of the experimental to the analytical data was used to confirm their representativeness.

Meshing the ABAQUS finite element analysis (FEA) consists of a network made up of nodes and cells. A wear simulation approach was created using global remeshing to mimic wear that is bigger than the elements of the FE mesh. A curvature control with maximum deviation factor 0.1 was chosen by fraction of global size 0.1. This was chosen to initiate the seeding process available or simply to start choosing the most compatible meshing nodes that could cover the whole area of entities. Finally, the job assignment and monitor phase to create the job load distribution results was used to ensure the successful execution of finite element simulations and error minimization.

## 3. Results

### *3.1 Definition of Critical and Catastrophic Wear Conditions*

In this study, critical operating conditions are defined as the maximum combinations of load and sliding speed at which stable sliding is maintained without excessive bending, loss of traction, or premature test termination. Beyond this regime, the rubber specimens exhibit rapid deformation, unstable contact, and severe material removal.

Catastrophic wear refers to abrupt failure characterised by chunk detachment, severe curvature of the rubber specimen, and loss of effective contact with the abrasive counterface. These events typically occurred within a few seconds of testing at the highest loads and speeds and represent the

practical operational limit of the material under MQWL conditions.

Wear resilience in this study is evaluated using the specific wear rate (mm³/N·m). It is found that the 30% improvement corresponds to the reduction in specific wear rate of DPNR-25 under MQWL conditions relative to its unlubricated condition. While 58% improvement corresponds to the further reduction in specific wear rate achieved by DPNR-50 compared with DPNR-25 under identical MQWL conditions. These results demonstrate that increasing carbon black content enhances load-carrying capability and resistance to abrasive wear, particularly in the presence of a thin water film that promotes cooling and debris removal during abrasion.

### *3.2 Comparison of Results for Lubricated and Unlubricated Conditions*

In lubricated sliding of DPNR-25, the trend shows that as the load gets higher, the weight loss increases with increasing speed as in Figure 3. Similar trend was observed for DPNR-25 in unlubricated conditions [1]. However, as the rubbing samples for the unlubricated conditions is 24 mm x 10 mm, bigger than in comparison to the lubricated conditions which is 10 mm x 10 mm, the samples in the unlubricated conditions could handle the load up to 35N; while only 15N load in lubricated conditions. This is due to the area under contact for lubricated conditioning is insufficient to fill up the gap between water film and the abrasive surface in contact causing deflation and sliding without good traction during the run. Hence, in lubricated conditions, a full traction contact area is needed to uphold the gripping between rubber and asphalt in real situations [19].

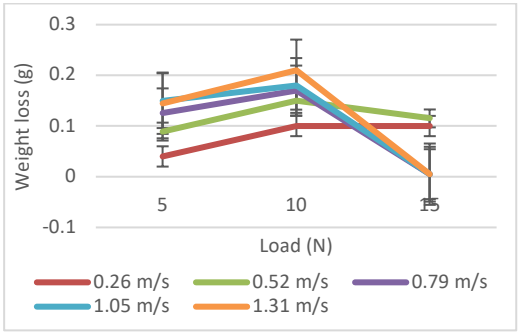


**Fig. 3.** Effect of load on weight loss at different speeds at DPNR 25 in lubricated conditions

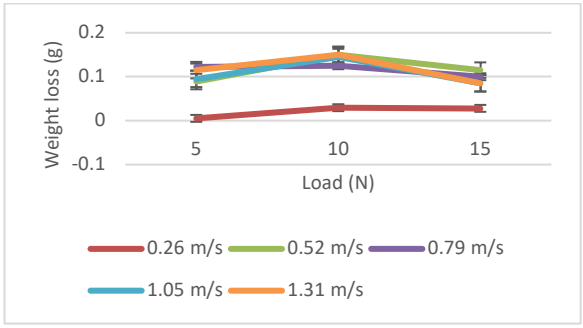


**Fig. 4**. Effect of load on weight loss at different speeds with DPNR 50 in lubricated conditions

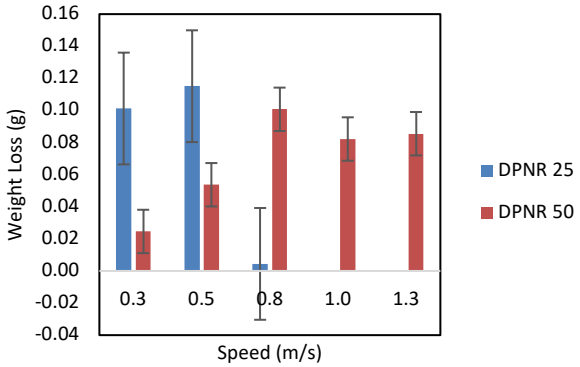


**Fig. 5**. Effect of weight loss at 15N in different speeds with different loading of CB in lubricated conditions

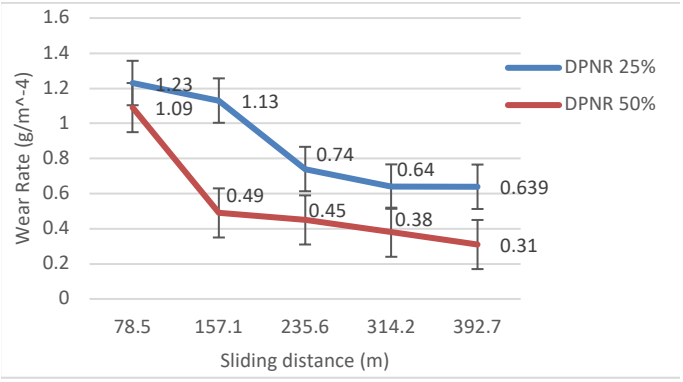


**Fig. 6.** Variation of wear rate of DPNR with different CB at different sliding distance at 10N in lubricated conditions

In Nasir and El-Tayeb. [1], it shows that DPNR-50 in unlubricated conditions could hold up to 35N too but only 25N in lubricated conditions as shown in Figure 4. It seems that both DPNR-25 and DPNR-50 in unlubricated conditions give comparable results corresponding to in lubricated conditions. It is likely to conclude that the weight loss increases with increases load and speed in both conditions but decreases as it reaches its critical condition.

In comparison, in Figure 5; for weight loss at 15N as the rubbing samples are bigger in unlubricated conditions (1.5 m/s), but in lubricated conditions it could handle maximum speed at to 0.7m/s for only 2 seconds. Nevertheless, the difference in percentage of weight loss for both lubricated and unlubricated conditions at 0.3 m/s are 60.9% and 2.4% respectively. Wear resistance in lubricated conditions is higher than in unlubricated conditions based on the area of contact geometry.

Comparing the wear rate of both DPNR-25 and DPNR-50 at 10N in both lubricated and unlubricated conditions as shown in Figure 4, the trendline shows the wear rate decreases when the sliding distance increases. Nevertheless, there is not much difference between the wear rate of DPNR-25 and DPNR-50 in unlubricated conditions but the trendline of Figure 6 shows a bigger gap. This is mainly due to in lubricated conditions the rubber experiences the dynamic properties of water thin film transference that created water run between the rubber surface and counter surfaces [20]. Comparing both SEM images gathered from [1] and results obtained, it is observed that there are differences in the sliding direction and formation of the rubber as shown in Figure 7(a) and (b) respectively. Presence of water and some impurities impacted the rubber surface shows the differences for both figures. However, the waves-like spacing were captured on the interface is similar, hence, applying the rubber wear abrasion and rolling occurred on the rubber surfaces before detachment.

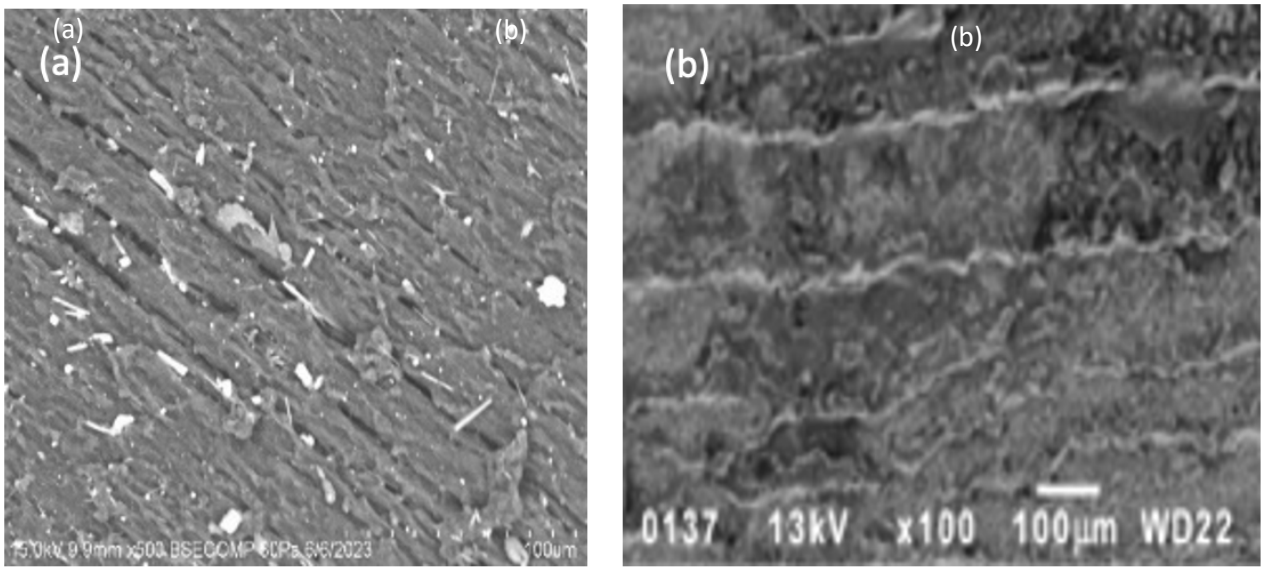


**Fig. 7.** SEM images of DPNR 25 in (a)lubricated and (b)unlubricated conditions

According to the Appendix A (Appendix A.1 and Appendix A.2) for DPNR-25 and DPNR-50 respectively, it is observed that the amount of water increases with increasing load and speed. This shows that good surface contact reduces the water entrapment in the running rubber surface and hence empowering the gripping to take place between the rubber surface. The formation of small spacing ridges reduces the water film in between the rubber and abrasive surfaces as the water receded inside the abrasive surface compartment [20]. The ridges can retain the minimum quantity of water inside them to enable the cooling effect, hence, reduce the elevated temperature to

maximum of not more than 25$^0$C (using IR temperature detector) during abrasion processes.

### *3.3 Effects of Load and Speed on Abrasive Wear*

The load and speed of this experiment correlate with each other where it gives impact on the abrasion of the rubber samples is shown in Figure 8. It is shown that the weight loss of DPNR-25 stops at 15N while DPNR-50 stops at 25N. To simplify, Figure 9(a) shows the data for DPNR 25 while Figure 9(b) shows DPNR 50. Here, the CB loading with 50mg is effective to elongate the usage in comparison to 25 mg, and hence it is reflected that the optimise CB loading is at 50mg. It is also noted that the effect of speed on wear for DPNR 25 is as shown in Figure 10 and for DPNR 50 in Figure 11, there is practical reduction in wear as the speed and load reduced as similarly stated by [1].

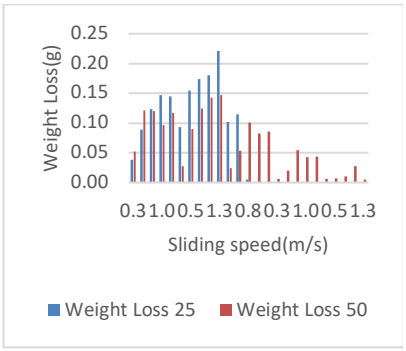


**Fig. 8.** Effect of speed on weight loss of DPNR at different CB

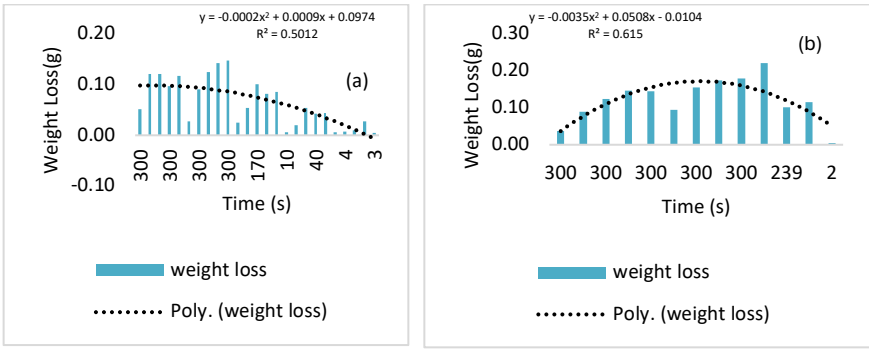


**Fig. 9**. Effect of speed on weight loss of (a) DPNR 25 (b) DPNR 50

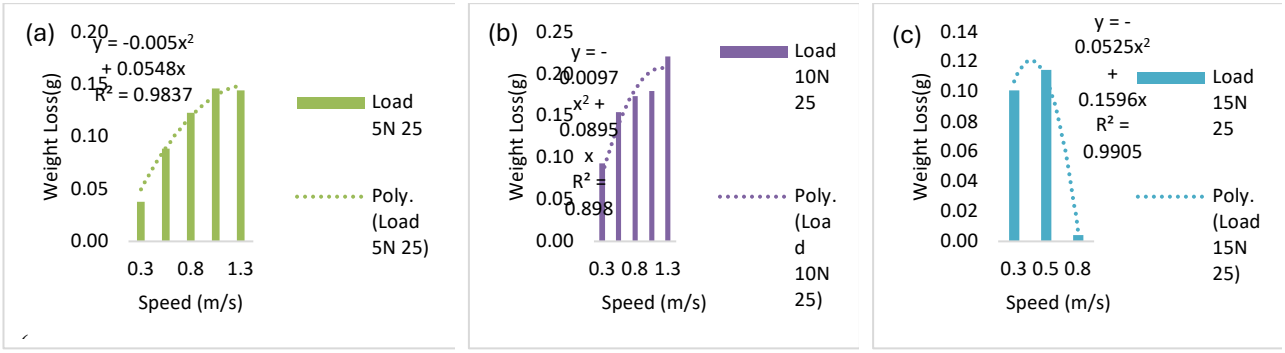


**Fig. 10.** Relationship between load (a) 5N, (b) 10N, (c) 15N, and speed with abrasive wear for DPNR 25

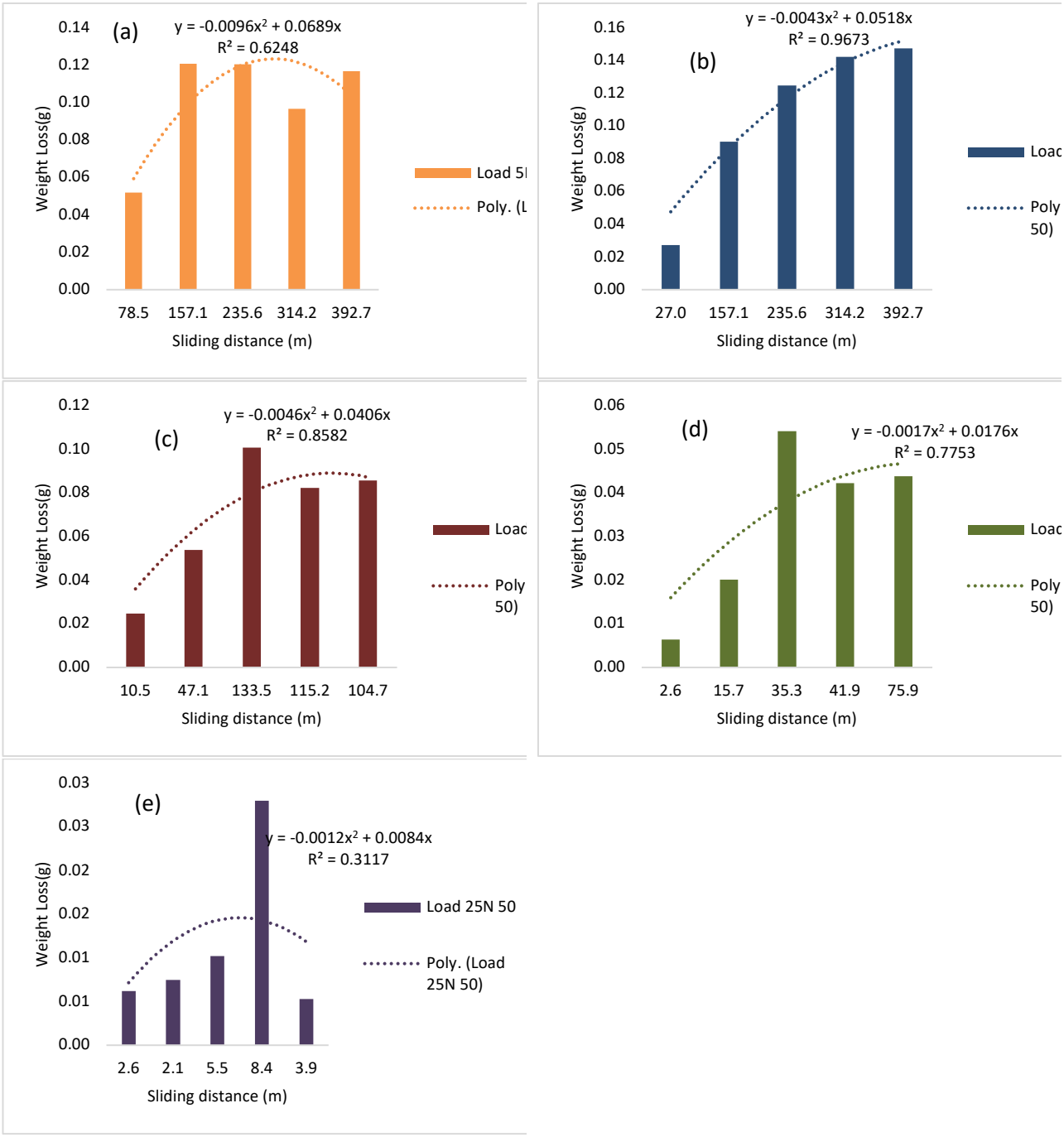


**Fig. 11**. Relationship between load (a) 5N, (b) 10N, (c) 15N, (d) 20N, (e) 25N and speed with abrasive wear for DPNR 50

It has also been observed in the Figures 12 and 13 respectively, the trendline increases at 5N and 10N while decrease drastically at 15N. This can be seen in Figure 13 where the trendline starts to increase indicating the weight loss increases with respect to time and speed and decreases when the time decreases at 239s and 2s. For Figures 14 and 15 prove that the trendline decreases due to the decrease in time for DPNR-50. In addition, when comparing both DPNR at the same speed of 1.3090m/s and at the same load of 5N, 5.6ml water was used throughout the 300s of the experiment for DPNR-25 while 10.6ml is used for DPNR-50. It is also observed that difference in CB also affecting the amount of water used for both samples.

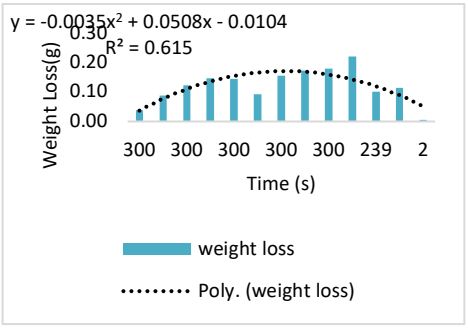


**Fig. 12.** Effect of time on weight loss of DPNR 25

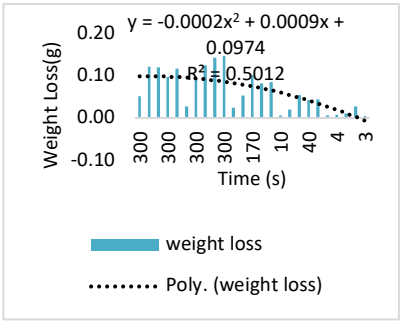


**Fig. 13.** Effect of time on weight loss of DPNR 50

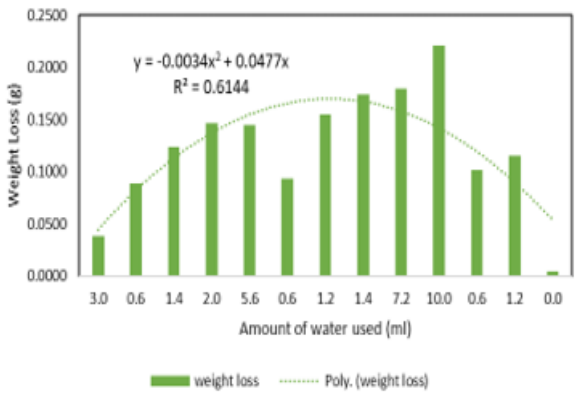


**Fig. 14.** Effect of the amount of water used on abrasive wear for DPNR 25

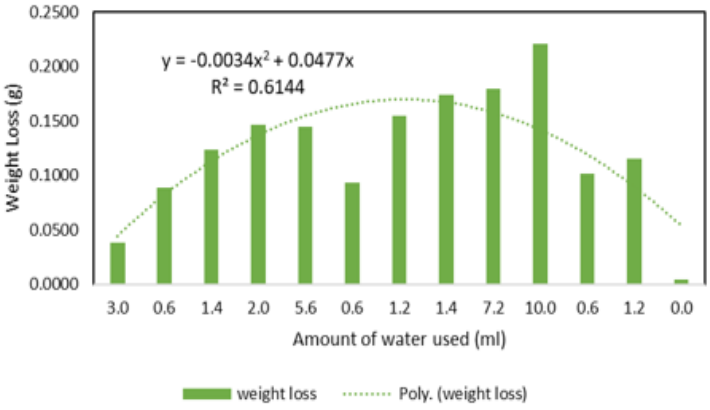


**Fig. 15.** Effect of the amount of water used on abrasive wear for DPNR 50

In Figs. 16(a) and (b) below show the SEM images of DPNR-25 and DPNR-50 tested at 5N, 0.2618m/s for 300s and 15N, 0.7854m/s for 2s, respectively. DPNR-50 exhibits superior wear resilience under MQWL conditions. Figure 16(a) image shows that the rubber has a roll formation type of wear. However, Figure 16(b) shows a chunk-like image since it only tested for 2s. Moreover, it is observed that during the experiments, the elasticity of the rubber samples at Figure 16(b) makes it curved drastically as soon as the experiment starts. Thus, it deteriorated and changes its rubbing samples from on top of the rubber samples surface to the side of the surface as the deflection occurred during the abrasion run [21].

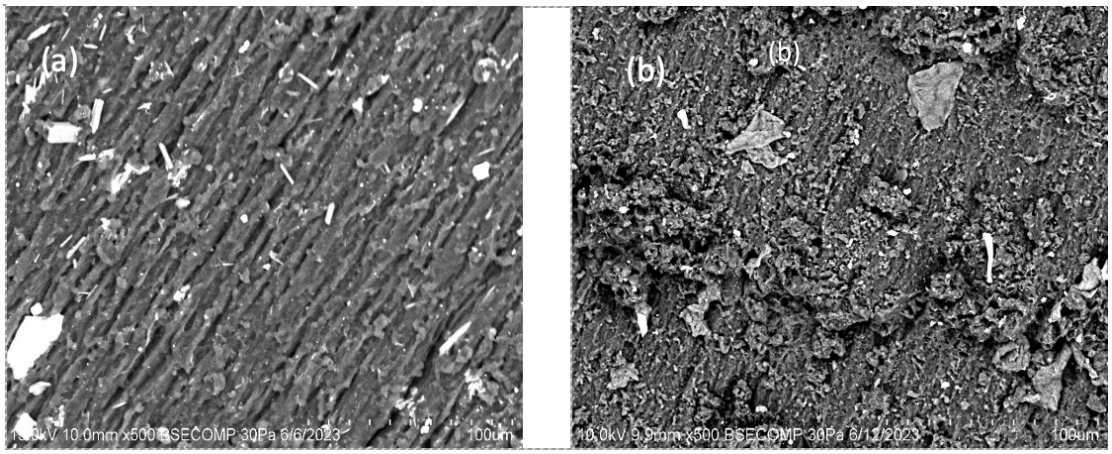


**Fig. 16.** SEM images of abraded surfaces of (a)DPNR 25 (b) DPNR 50 at 5N,0.2618m/s

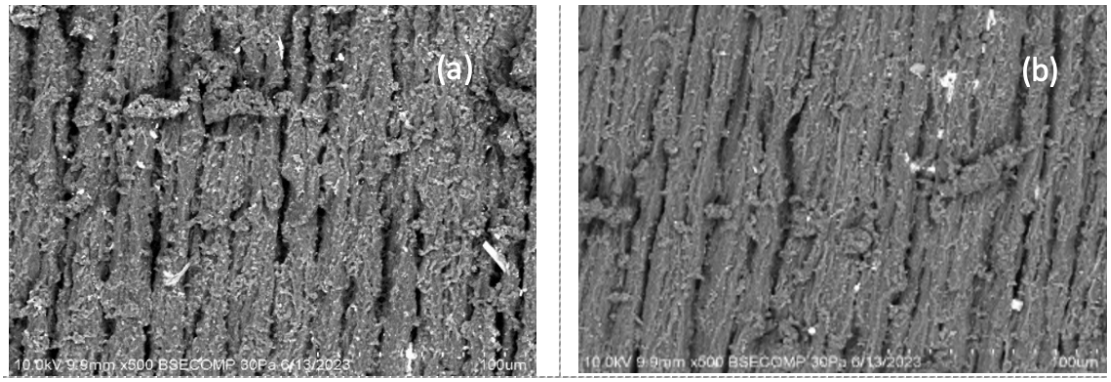


**Fig. 17.** SEM/EDX of abraded surfaces of (a)DPNR 25 and (b)DPNR50

Comparing Figs. 17(a) and (b), with the same rubbing surfaces for both rubber samples underwent curving effect by bending sideways during the experiment for DPNR-50 at 20N, 0.2618m/s for 10s and 25N, 0.7854m/s for 7s, respectively. It appears that both figures show roll formation and stuck wear debris occurred [22]. Elemental compositions present in the DPNR-25 and DPNR-50 are as shown in Figure 17. The elements present in both samples such as carbon, sulphur, oxygen, sodium, chlorine, zinc are confirmed in the DPNR according to Table 1.

### *3.4 Simulated FEA Results Based on DPNR 50 As Rubber Tire Performance*

The finite element analysis (FEA) was conducted to qualitatively assess the deformation behaviour and safety margin of a tyre-scale rubber structure under high load conditions. The simulation does not directly predict wear rates but instead evaluates displacement, contact interaction, and structural response under loading scenarios representative of aggressive riding or burnout conditions.

The safety factor contours generated in Abaqus represent relative deformation severity, with blue zones indicating low deformation risk and red zones indicating critical deformation. The reported load range of approximately 1453–1598 N corresponds to the maximum applied loads before excessive deformation occurred in the simulated tyre model. These values are used to indicate deformation thresholds rather than direct failure loads and are discussed in relation to experimental observations of specimen deflection and instability in PoD testing.

The simulation of the DPNR 50 rubber surface on the displacement versus time was performed to assess the ability of the simulated rubber tire for motorcycle on asphalt to integrate the real situation as depicted in Figure 18(a). In Figure 18(b), the graph shown above only depicts tire displacement on z-axis which is perpendicular to the force applied. As referred from the horizontal linear line, the gravitational force is kept constant throughout the running in counter-surface contact which is relatable as rider and motorcycle weight does not change during riding experience as mentioned by Edeskär [15].

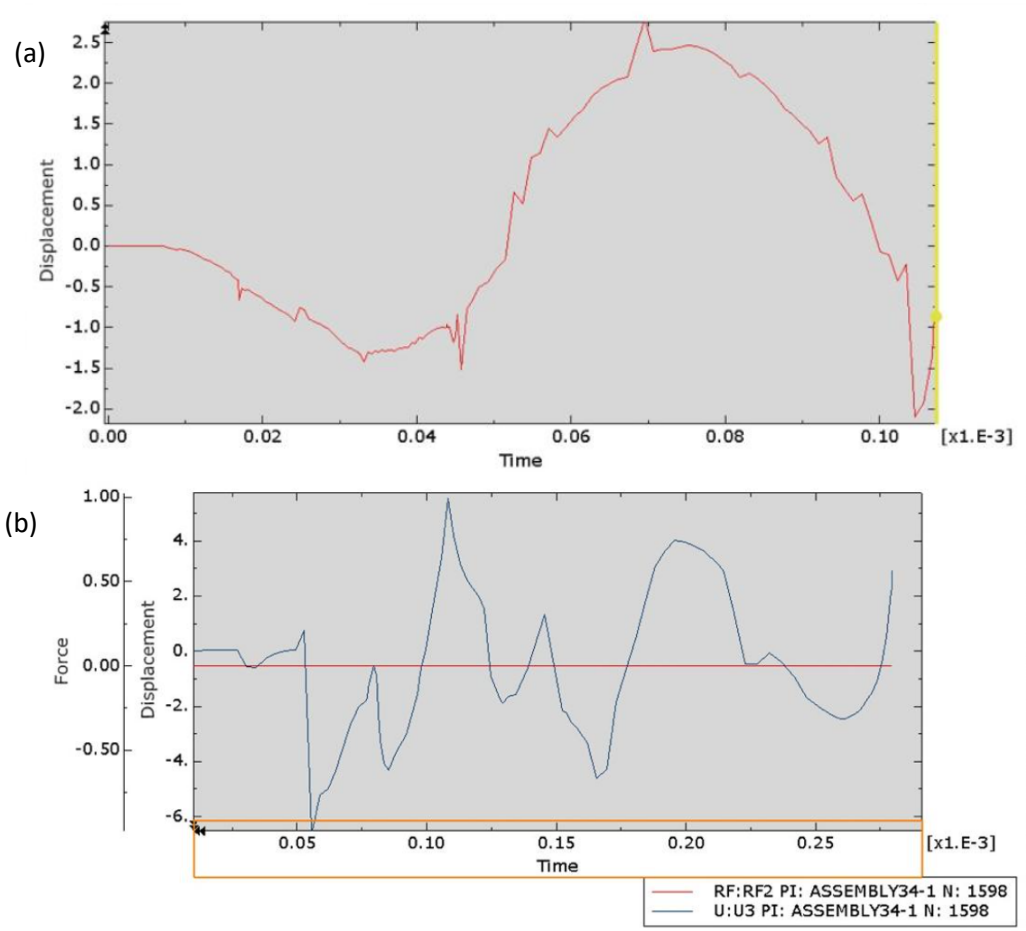


**Fig. 18.** Displacement over Time for (a) normal and (b) burnout conditions

In comparing the two different riding experiences, the burnout incident is more obvious and aggressive displacement than the normal riding experience as it involves more friction on the tire due to loading process with maximum load at 1453-1598 N as shown in Simulation Abaqus in Figures 19 to 21 below.

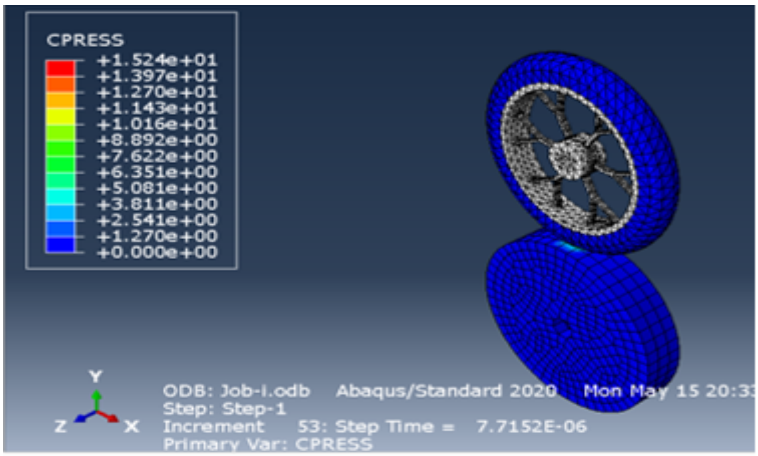


**Fig. 19.** Model for maximum loading at 1524N

In determining the safety factor, the resulting animation could be observed to inspect the maximum magnitude that the tire could handle. Series of colours starting from blue up to red depict the level of magnitude change with the red one being the most extreme displacement onto the tire

[12] as shown in Figures 20 and 21.

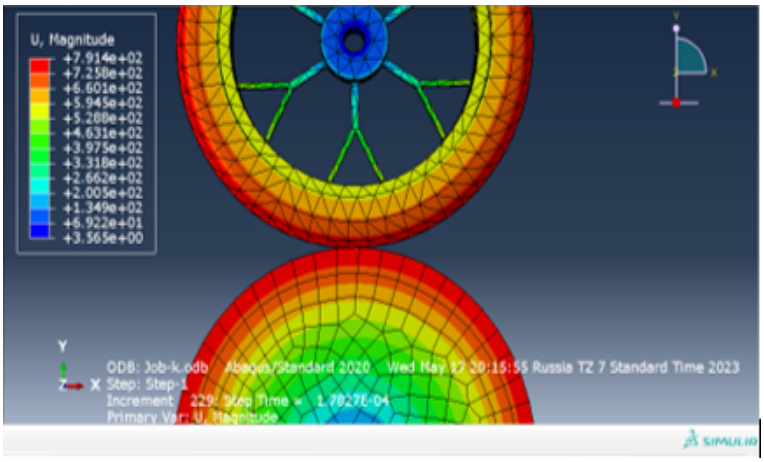


**Fig. 20.** The safety factor animates with max magnitude

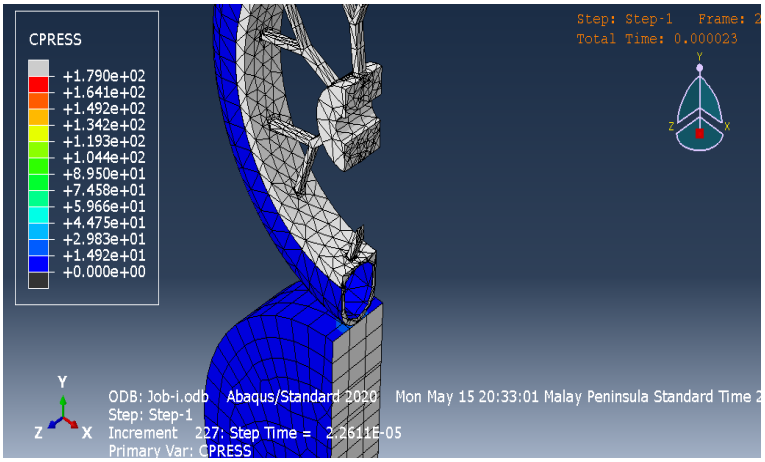


**Fig. 21.** Cross-sectional view of tire during simulation

## 4. Discussion

The wear and friction behaviour have been monitored, and they show similarity to the experimental results expected from the elastomeric properties. The minimum amount of water used to cool down the DPNR rubber has been observed as the maximum temperature is at $25^0$C. The concentration of Carbon black (CB) also affected the wear and friction associated with DPNR rubber. Load and sliding distance have become a major parameter to be observed as the DPNR rubber seems start to curve drastically at 25N load. Further investigation was undertaken to determine the FEA on DPNR-50 for validation result. It can be observed from the results that the displacement slowly reduced before it increases to almost 2.5 mm max displacement occurred at 6.54 x $10^{-5}$ N Umagnitude(red zone) and starting to reduce to the lowest –2.0 mm displacement before it stops. This gives us the insight that the displacement has taken place for the tires to run smoothly after overcoming the initial force and upon breaking it releases maximum force and stops has also been discussed by Molero *et al*., [13], Elalem *et al*., [22] and Klüppel *et al*., [26]. A modern tire now has roughly 25 different parts. They are textiles, steel, and rubber. However, DPNR 50 rubber accounts for up to 40 wt.% of the total as designed [23]. Accordingly, Gent *et al*., [24] and Zhang *et al*., [25] agreed the composition of modern tires could vary depending on the use for which they were designed. As shown in Figures 18 and 19, the shade of colour green is set to be the safety factor

determined automatically by the software with the magnitude value of $5.288x10^2$N Umagnitude to be the upper limit of magnitude that could be applied to the tire before entering the red zone as supported by Cossalter *et al*., [20], Klüppel *et al*., [26] and Arib *et al*., [27] previously. Despite the insights obtained, several limitations of the present study are acknowledged. The PoD tests were conducted over relatively short durations and simplified contact geometries, which cannot fully replicate long-term tyre wear under variable road conditions. The MQWL approach represents an idealised lubrication scenario and does not account for contaminants, temperature gradients, or complex hydrodynamic effects encountered in real service. Additionally, the FEA model employed simplified material properties and geometry, limiting its predictive capability. Future work will focus on extended-duration wear testing, incorporation of temperature-dependent viscoelastic material models, and more detailed tyre geometries including tread patterns and composite reinforcement layers. Coupled thermo-mechanical simulations will also be explored to better represent real tyre operating environments.

## 5. Conclusions

The abrasive wear behaviour of deproteinised natural rubber under MQWL conditions was systematically investigated. Wear increased with increasing load and sliding speed but stabilised near critical operating conditions of 15 N for DPNR-25 and 25 N for DPNR-50 prior to catastrophic wear. Compared with unlubricated conditions, DPNR-25 exhibited a 30% improvement in wear resilience under MQWL, while DPNR-50 demonstrated a further 58% improvement relative to DPNR-25, achieving a minimum specific wear rate of 0.05 $mm^3/N{\cdot}m$. The FEA provided qualitative insight into deformation behaviour and safety margins at the tyre scale, supporting the experimental observation that higher carbon black content enhances structural stability under high loads. These findings contribute to improved understanding of rubber wear mechanisms and provide guidance for the design of more durable tyre compounds under lubricated or wet operating conditions.

**Author Contributions:**"Conceptualization, R.M.N.; methodology, R.M.N. & N.A.A.M..; software, M.F.A..; validation, R.M.N., N.A.A.M. and M.F.A.; writing—review and editing, R.M.N.; supervision, R.M.N. All authors have read and agreed to the published version of the manuscript."

**Funding:** This research was funded by the Ministry of Higher Education under grant no. FRGS/1/2020/TK0/USM/02/37(203.PMEKANIK.6071486) and Universiti Sains Malaysia (USM) for providing the financial support.

**Acknowledgments:** Many thanks to the administrative and technical support from USM, and donations in kind (materials and some mechanical testing used for the experiments) from MRB, Malaysia. The authors have reviewed and edited the output and take full responsibility for the content of this publication.

**Conflicts of Interest:** The authors declare no conflicts of interest. The funders had no role in the design of the study; in the collection, analyses, or interpretation of data; in the writing of the manuscript; or in the decision to publish the results.

## Abbreviations

The following abbreviations are used in this manuscript:

| | |
|---|---|
| CB | Carbon black |
| DPNR | Deproteinised Natural Rubber |
| MQWL | Minimum Quantity Water Lubricated |
| SEM | Scanning Electron Microscopy |
| EDX | Energy Dispersive X-ray Spectroscopy |
| FEA | Finite Element Analysis |
| SBR | Styrene butadiene rubber |
| NR | Natural rubber |
| DPNR 25 | Deproteinised natural rubber with 25wt.% Carbon black |
| DPNR 50 | Deproteinised natural rubber with 50wt.% Carbon black |
| MRB | Malaysia Rubber Board |
| POD | Pin-on Disc |
| ASTM | American Society for Testing and Materials |
| SR | Single roller |
| HP | Horsepower |
| SLDPRT | Solid Part |

## References

[1] Nasir, R. M., and N. S. M. El-Tayeb. "Surface morphology, mechanical and tribological properties of blended deproteinized natural and polyisoprene rubbers." *Journal of Thermoplastic Composite Materials* 25, no. 6 (2012): 701-715. https://doi.org/10.1177/0892705711412812

[2] Nishi, Toshiaki. "Rubber wear mechanism discussion based on the relationship between the wear resistance and the tear resistance with consideration of the strain rate effect." *Wear* 426 (2019): 37-48. https://doi.org/10.1016/j.wear.2018.12.084

[3] Friedrich, K., H. J. Sue, P. Liu, and A. A. Almajid. "Scratch resistance of high performance polymers." *Tribology International* 44, no. 9 (2011): 1032-1046. https://doi.org/10.1016/j.triboint.2011.04.008

[4] Wu, Y. P., Y. Zhou, J. L. Li, H. D. Zhou, J. M. Chen, and H. C. Zhao. "A comparative study on wear behavior and mechanism of styrene butadiene rubber under dry and wet conditions." *Wear* 356 (2016): 1-8. https://doi.org/10.1016/j.wear.2016.01.025

[5] Wu, Guangchang. "The mechanisms of rubber abrasion." PhD diss., Queen Mary University of London, 2017.

[6] Sharifah Allyana, S. M. R., H. Z. Zarir, A. M. Abdul Rahmat, M. F. Siti Atiqah, F. P. Noor, S. V. Wong, and M. J. Jamilah. "Recent trend of fatal motorcycle crashes in Malaysia." In *of the 8th International Forum of Automotive Traffic Safety (INFATS)*. 2010.

[7] Chandelia, Vijay Kisan, Hung-Jue Sue, and Mohammad Motaher Hossain. "FEM modeling on scratch behavior of multiphase polymeric systems." *Tribology Letters* 66, no. 2 (2018): 62. https://doi.org/10.1007/s11249-018-1012-3

[8] Odabas, D. "Effects of load and speed on wear rate of abrasive wear for 2014 Al alloy." In *IOP conference series: materials science and engineering*, vol. 295, no. 1, p. 012008. IOP Publishing, 2018. https://doi.org/10.1088/1757-899X/295/1/012008

[9] Rejab, M. N. A., R. A. Rahman, R. I. R. Hamzah, J. I. I. Hussain, N. Ahmad, A. Ismail, and A. Putra. "Fabricating process and mechanical properties of elastomeric mount." In *the 7th South East Asia Technical University Consortium Symposium Institut Teknologi Bandung, Bandung, Indonesia*, pp. 4-6. 2013. https://www.researchgate.net/publication/316697484_Effect_of_carbon_black_fillers_on_tensile_stress_of_unvulcanized_natural_rubber_compound [accessed Feb 25 2025].

[10] Hakami, Ferial, A. Pramanik, N. Ridgway, and A. K. Basak. "Developments of rubber material wear in conveyer belt system." *Tribology International* 111 (2017): 148-158. https://doi.org/10.1016/j.triboint.2017.03.010

[11] Arias, Sergio G. "Finite Element Analysis of Rubber Treads on Tracks to Simulate Wear Development." In *3DS Simulia Community Conference*. 2012.

[12] Behera, A., The influence of tire temperature and velocity on vehicle dynamics. Technical Report, October 2019 (2019): 1-38, Available in https://www.researchgate.net/publication/344777324

[13] Molero, Glendimar, and Hung-Jue Sue. "Scratch behavior of model epoxy resins with different crosslinking densities." *Materials & Design* 182 (2019): 107965.https://doi.org/10.1016/J.MATDES.2019.107965

[14] Rosszainily, I. R. A., M. A. Salim, M. R. Mansor, M. Z. Akop, A. Putra, M. T. Musthafah, M. Z. Hassan, MN Abdul Rahman, and M. N. Sudin. "Effect of carbon black fillers on tensile stress of unvulcanized natural rubber compound." *Journal of Mechanical Engineering and Sciences* 10, no. 2 (2016): 2043-2052. https://doi.org/10.15282/jmes.10.2.2016.9.0193

[15] Edeskär, Tommy. *Technical and environmental properties of tyre shreds focusing on ground engineering applications*. Luleå tekniska universitet, 2004.(PDF) Technical and Environmental Properties of Tyre Shreds Focusing on Ground Engineering Applications

[16] Motorcycle Dynamometer | Hyper Power. (n.d.). Retrieved May 18, (2023), from https://www.hyper-power.net/index.php/dynamometers/bike/motorcycle-dynamometer.html

[17] F1 tires: What are the compounds and what do they mean? Retrieved December 15, (2022), from https://www.autosport.com/f1/news/f1-tires-what-are-the-compounds-and-what-do-they-mean/10344284/

[18] Wu, Jian, Long Chen, Da Chen, Youshan Wang, Benlong Su, and Zhibo Cui. "Experiment and simulation research on the fatigue wear of aircraft tire tread rubber." *Polymers* 13, no. 7 (2021): 1143.https://doi.org/10.3390/POLYM13071143

[19] Asphalt Concrete | Density, Strength, Melting Point, Thermal Conductivity. Retrieved January 20, (2023), Available from https://material-properties.org/asphalt-concrete-density-strength-melting-point-thermal-conductivity/

[20] Cossalter, Vittore, Alberto Doria, Roberto Lot, N. Ruffo, and M. Salvador. "Dynamic properties of motorcycle and scooter tires: measurement and comparison." *Vehicle system dynamics* 39, no. 5 (2003): 329-352.https://doi.org/10.1076/VESD.39.5.329.14145

[21] El-Tayeb, N. S. M., and R. Md Nasir. "Effect of soft carbon black on tribology of deproteinised and polyisoprene rubbers." *Wear* 262, no. 3-4 (2007): 350-361. https://doi.org/10.1016/j.wear.2006.05.021

[22] Elalem, Khaled, and D. Y. Li. "Dynamical simulation of an abrasive wear process." *Journal of computer-aided materials design* 6, no. 2 (1999): 185-193.

[23] Park, Byung-Ho, Dong-Ho Chang, Han-Seok Song, Il-taik Jung, and Choon-Tack Cho. "Design concept of tread compound for cutting and chipping resistance of truck tyres on on/off the roads." *Asian Journal of Chemistry* 25, no. 9 (2013): 5208. https://doi.org/10.14233/ajchem.2013.F21

[24] Gent, Alan Neville, and Joseph D. Walter. "Pneumatic tire." (2006). Pneumatic Tire,

[25] Zhang, Qijun, Jiawei Yin, Zeping Cao, Tiange Fang, Jianfei Peng, Lin Wu, and Hongjun Mao. "Size distribution, chemical composition and influencing factors of vehicle tire wear particles based on a novel test cycle." *Environmental Research* 268 (2025): 120817. https://doi.org/10.1016/j.envres.2025.120817

[26] Klüppel, M. Wear and Abrasion of Tires. (2014): 1-6 In: Kobayashi, S., Müllen, K. (eds) Encyclopedia of Polymeric Nanomaterials. Springer, Berlin, Heidelberg, https://doi.org/10.1007/978-3-642-36199-9_312-1

[27] Arib Rejab, M. N., S. A. Abdul Shukor, M. R. Mohd Sofian, J. I. Inayat-Hussain, A. Nazirah, and I. Asyraf. "Evaluation of the effectiveness of elastomeric mount using vibration power flow and transmissibility methods." In *Journal of Physics: Conference Series*, vol. 908, no. 1, p. 012034. IOP Publishing, 2017. doi:10.1088/1742-6596/908/1/012034

## Appendix A

*Appendix A.1*

| Sample | Load (N) | Weight Loss (mg) | Volume Loss (mm^3) | Sliding Distance(m) | Time (s) | Wear Rate (mm^3/m) | Specific WR (mm^3/Nm) | sliding speed (m/s) | amount of water(ml) |
|---|---|---|---|---|---|---|---|---|---|
| R1 | 5 | 0.04 | 38.2 | 78.5 | 300 | 0.49 | 0.10 | 0.26 | 3.0 |
| R2 | 5 | 0.09 | 87.3 | 157.1 | 300 | 0.56 | 0.11 | 0.52 | 0.6 |
| R3 | 5 | 0.12 | 133.5 | 235.6 | 300 | 0.57 | 0.11 | 0.79 | 1.4 |

| | | | | | | | | | |
|---|---|---|---|---|---|---|---|---|---|
| R4 | 5 | 0.15 | 144.1 | 314.2 | 300 | 0.46 | 0.09 | 1.05 | 2.0 |
| R5 | 5 | 0.14 | 170.0 | 392.7 | 300 | 0.43 | 0.09 | 1.31 | 5.6 |
| R6 | 10 | 0.09 | 96.7 | 78.5 | 300 | 1.23 | 0.12 | 0.26 | 0.6 |
| R7 | 10 | 0.15 | 178.1 | 157.1 | 300 | 1.13 | 0.11 | 0.52 | 1.2 |
| R8 | 10 | 0.17 | 173.5 | 235.6 | 300 | 0.74 | 0.07 | 0.79 | 1.4 |
| R9 | 10 | 0.18 | 201.7 | 314.2 | 300 | 0.64 | 0.06 | 1.05 | 7.2 |
| R10 | 10 | 0.22 | 251.2 | 392.7 | 300 | 0.64 | 0.06 | 1.31 | 10.0 |
| R11 | 15 | 0.10 | 100.0 | 62.6 | 239 | 1.60 | 0.11 | 0.26 | 0.6 |
| R12 | 15 | 0.12 | 121.8 | 1.0 | 2 | 116.29 | 7.75 | 0.52 | 1.2 |
| R13 | 15 | 0.00 | 4.3 | 1.6 | 2 | 2.77 | 0.18 | 0.79 | 0.0 |

## *Appendix A.2*

Sample R31-R55 for DPNR 50

| Sample | Load (N) | Weight Loss (mg) | Volume Loss (mm^3) | Sliding Distance (m) | Time (s) | Wear Rate (mm^3/m) | Specific WR (mm^3/Nm) | sliding speed (m/s) | amount of water (ml) |
|---|---|---|---|---|---|---|---|---|---|
| R31 | 5 | 0.05 | 46.7 | 78.5 | 300 | 0.59 | 0.12 | 0.26 | 0.8 |
| R32 | 5 | 0.12 | 101.7 | 157.1 | 300 | 0.65 | 0.13 | 0.52 | 2.2 |
| R33 | 5 | 0.12 | 107.5 | 235.6 | 300 | 0.46 | 0.09 | 0.79 | 4.4 |
| R34 | 5 | 0.10 | 92.7 | 314.2 | 300 | 0.30 | 0.06 | 1.05 | 2.4 |
| R35 | 5 | 0.12 | 98.1 | 392.7 | 300 | 0.25 | 0.05 | 1.31 | 10.6 |
| R36 | 10 | 0.03 | 29.5 | 27.0 | 103 | 1.09 | 0.11 | 0.26 | 0.4 |

| | | | | | | | | | |
|---|---|---|---|---|---|---|---|---|---|
| R37 | 10 | 0.09 | 77.5 | 157.1 | 300 | 0.49 | 0.05 | 0.52 | 1 |
| R38 | 10 | 0.12 | 106.6 | 235.6 | 300 | 0.45 | 0.05 | 0.79 | 1.8 |
| R39 | 10 | 0.14 | 118.8 | 314.2 | 300 | 0.38 | 0.04 | 1.05 | 4.2 |
| R40 | 10 | 0.15 | 121.9 | 392.7 | 300 | 0.31 | 0.03 | 1.31 | 3.2 |
| R41 | 15 | 0.02 | 23.0 | 10.5 | 40 | 2.19 | 0.15 | 0.26 | 0.4 |
| R42 | 15 | 0.05 | 47.7 | 47.1 | 90 | 1.01 | 0.07 | 0.52 | 0.6 |
| R43 | 15 | 0.10 | 86.4 | 133.5 | 170 | 0.65 | 0.04 | 0.79 | 3 |
| R44 | 15 | 0.08 | 76.0 | 115.2 | 110 | 0.66 | 0.04 | 1.05 | 3.8 |
| R45 | 15 | 0.09 | 79.8 | 104.7 | 80 | 0.76 | 0.05 | 1.31 | 2.6 |
| R46 | 20 | 0.01 | 5.9 | 2.6 | 10 | 2.24 | 0.11 | 0.26 | 0.8 |
| R47 | 20 | 0.02 | 16.8 | 15.7 | 30 | 1.07 | 0.05 | 0.52 | 0.6 |
| R48 | 20 | 0.05 | 46.9 | 35.3 | 45 | 1.33 | 0.07 | 0.79 | 1.8 |
| R49 | 20 | 0.04 | 38.4 | 41.9 | 40 | 0.92 | 0.05 | 1.05 | 3 |
| R50 | 20 | 0.04 | 38.2 | 75.9 | 58 | 0.50 | 0.03 | 1.31 | 3.6 |
| R51 | 25 | 0.01 | 6.0 | 2.6 | 10 | 2.29 | 0.09 | 0.26 | 0.4 |
| R52 | 25 | 0.01 | 6.7 | 2.1 | 4 | 3.18 | 0.13 | 0.52 | 0.4 |
| R53 | 25 | 0.01 | 8.3 | 5.5 | 7 | 1.51 | 0.06 | 0.79 | 0.2 |
| R54 | 25 | 0.03 | 23.0 | 8.4 | 8 | 2.75 | 0.11 | 1.05 | 0.2 |
| R55 | 25 | 0.01 | 5.2 | 3.9 | 3 | 1.33 | 0.05 | 1.31 | 0.2 |